Chem Soc Rev

REVIEW ARTICLE

Doped graphene for metal-free catalysis

Xiang-Kai Kong,[a] Chang-Le Chen*[b] and Qian-Wang Chen*[ac]

Cite this: DOI: 10.1039/c3cs60401b

Received 6th November 2013

DOI: 10.1039/c3cs60401b

www.rsc.org/csr

Graphene has attracted increasing attention in different scientific fields including catalysis. *Via* modification with foreign metal-free elements such as nitrogen, its unique electronic and spin structure can be changed and these doped graphene sheets have been successfully employed in some catalytic reactions recently, showing them to be promising catalysts for a wide range of reactions. In this review, we summarize the recent advancements of these new and interesting catalysts, with an emphasis on the universal origin of their catalytic mechanisms. We are full of hope for future developments, such as more precisely controlled doping methods, atom-scale surface characterization technology, generating more active catalysts *via* doping, and finding wide applications in many different fields.

1. Introduction

Catalysis is an important phenomenon ubiquitous in nature as well as in artificial chemical transformations. It is not only one of the hottest topics in academic research, but also affects the chemical industry and changes our lives much more profoundly than we realize. Without molecular sieve catalysts for the conversion of methanol to gasoline, mankind would be confronted with a serious shortage of energy. The synthesis of ammonia *via* heterogeneous catalysis using a K-promoted iron oxide system has helped to resolve the food production problem. Supereminent activity and high selectivity are the prerequisite of catalysts, which can accelerate the chemical reactions and save the undesired consumption of reactants. In addition, good stability, convenience for recycling and low toxicity are also desirable properties for various catalysts.

[a] *Hefei National Laboratory for Physical Sciences at Microscale and Department of Materials Science & Engineering, University of Science and Technology of China, Hefei, China. E-mail: cqw@ustc.edu.cn; Fax: +86 551 63603005; Tel: +86 551 63603005*

[b] *CAS Key Laboratory of Soft Matter Chemistry and Department of Polymer Science & Engineering, University of Science and Technology of China, Hefei, China. E-mail: changle@ustc.edu.cn*

[c] *CAS High Magnetic Field Laboratory, University of Science and Technology of China, China & Collaborative Innovation Center of Suzhou Nano Science and Technology, China*

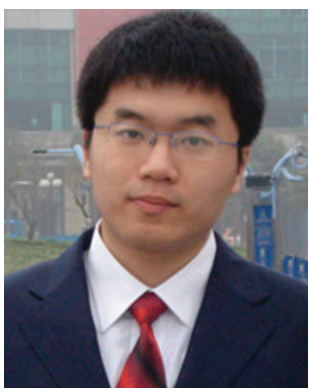

Xiang-Kai Kong

Xiang-Kai Kong completed his BS degree in Materials Physics from Huaibei Normal University in 2009. He is currently pursuing his PhD under the guidance of Professor Qian-Wang Chen at the University of Science and Technology of China. His research interests include catalysis, carbon materials, surface enhanced Raman scattering and theoretical simulations.

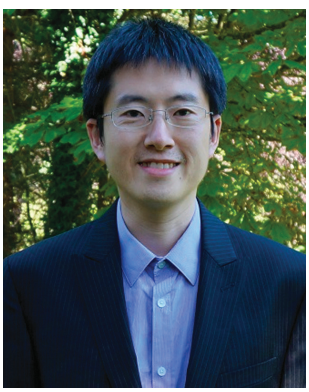

Chang-Le Chen

Chang-Le Chen is currently a Professor in the Department of Polymer Science and Engineering at the University of Science and Technology of China in Hefei, China. Chang-Le obtained his BS degree from USTC, and his MS and PhD degrees from University of Chicago under the supervision of Prof. Richard Jordan. Before taking his faculty position, he did a postdoc study at Northwestern University with Prof. Tobin Marks, and worked as a Scientist II at Celanese Corporation. His notable awards include Albert J. Cross Prize, American Chemical Society DIC Young Investigator Award, IUPAC Prizes-Honorable Mention and the Recruitment Program of Global Experts.

Metallic nanoparticles are undoubtedly the most vibrant catalysts due to their good performance in a series of paramount chemical reactions in modern chemistry. However, their use on an industrial scale is restricted by limited reserves, high cost and low stability. In the drive towards green and sustainable chemistry, carbon nanomaterials without metal elements have been explored and studied extensively in catalysis.[1] Labeled as metal-free catalysts, carbon nanomaterials have attracted more and more attention due to their fine performance in some chemical reactions, such as oxygen reduction reaction in fuel cells,[2–6] oxidative dehydrogenation,[7–11] oxidation of various alcohols and hydration of different alkynes,[12] reduction of nitrobenzene[13] and oxidant of thiols and sulfides.[14] It is generally accepted that carbon nanostructures are mainly classified into three categories: (1) 2D graphene, with completely flat sp^2 hybridizations, being of good conductivity and seminal catalytic function; (2) 1D carbon nanotubes and nanofibers with high strength; and (3) 0D fullerene with good semiconductor properties. The latter two allotropes are constructed by curved sp^2 hybridizations, whose π orbitals contain a certain amount of s electrons in addition to p electrons. Here, this review will focus on graphene, which is assembled by planar sp^2 hybrid carbon atoms with the s, p_x and p_y atomic orbitals on each carbon atom forming three strong σ bonds with the three surrounding atoms.[15]

Graphene, which is composed of one monolayer of carbon atoms with a honeycomb structure, has attracted considerable interest among the public because of its unique electronic, optical, thermal, and mechanical properties. It is a zero band gap semiconductor with the valence and conduction bands touching at the Brillouin zone corners.[16] High-quality graphene can be prepared by various methods including micro mechanical exfoliation, epitaxial growth and chemical vapor deposition (CVD). However, the zero band gap property weakens its catalytic activity and limits its broader applications.[17,18]

Qian-Wang Chen

Professor Qian-Wang Chen received his PhD from the University of Science and Technology of China (USTC) in 1995 and was appointed to the faculty of USTC. Later, he worked as a post doctoral researcher in the Institute of Hydrothermal Chemistry, Kochi, Japan, Alexander von Humboldt Research Fellow in Solar Energy Institute of Hannover, Germany and visiting researcher in the Hong Kong Polytechnic University. He was appointed as a professor in 2000 at the USTC and was awarded the Cheung Kong Professorship in 2002 by the Ministry of Education of China. His research interests include the synthesis and application of nanoscale materials.

Fortunately, the introduction of heteroatoms into graphene presents the potential to tweak its electronic and electrochemical properties by changing the electronic density within the graphene sheet.[19] Accordingly, doping with foreign non-metallic atoms has been demonstrated both experimentally and theoretically as a successful method to tune graphene's electronic structure, increasing active sites and enhancing catalytic activity significantly. However, much of the research in this field is still in its infancy. Some groups have reviewed the applications of graphene-based materials in catalysis, however the authors only lay emphasis on the graphene–metal/metal oxide nanocomposite catalysts[1,18,20,21] and oxygen reduction reactions.[3,20–23]

In this review, we will discuss the latest advances in the catalytic chemistry of doped graphene, which has been considered as one of the most promising metal-free catalysts, with the hope of increasing the awareness of this novel catalyst and stimulating further exploration of its applications in more reactions. The reports of different doped graphenes are introduced according to the type of the doping element. Foreign O element is usually attached to the respective materials in the hydroxyl and carboxyl forms, not a doping format in a strict sense. However, it is still a metal-free modification, similar to the doping structure. Moreover, it is the origin of graphene-related materials employed as metal-free catalysts in synthetic applications[12] and is often used as the precursor for other heteroatom doping. Additionally, the oxygenated groups are inevitable in graphene-based materials and cannot be completely removed during the reduction process, making its catalytic properties very important in this discussion. In each element doping section, the existing synthetic method will be introduced briefly and readers can refer to previous reviews if required to get more detailed preparation information.[15,18,24] Then, the progress of both experimental and theoretical investigations will be discussed. Finally, a brief summary and an outlook on the future development of doped graphene in catalysis will be presented.

2. Graphene-functionalized with foreign elements

2.1. O-attached graphene (χ = 3.44)

Oxygen heteroatoms are often unavoidable in graphene, especially when it is obtained from the classic Hummers method owing to the employment of strong oxidizing agent. Even after sufficient reduction, these attached oxygen functional groups are inevitable and cannot be completely removed. Graphene oxide (GO) is usually synthesized by exfoliation of graphite oxide obtained by the oxidation of natural graphite powder with various oxidants in acidic media[18] (Hummers method). It is frequently used as the precursor to prepare graphene and could be regarded as a typical O-attached graphene. Although the precise atomic and electronic structures of GO remain largely unknown, as a simplified model, it can be depicted as individual graphene sheets decorated with abundant oxygen

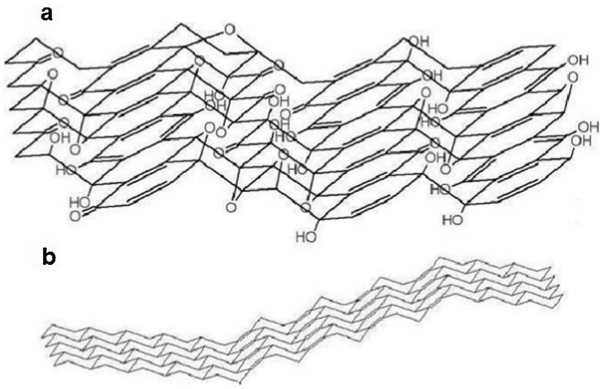

Fig. 1 A new structure model of GO: (a) surface species and (b) folded carbon skeleton. With permission from ref. 26, copyright 2006, American Chemical Society.

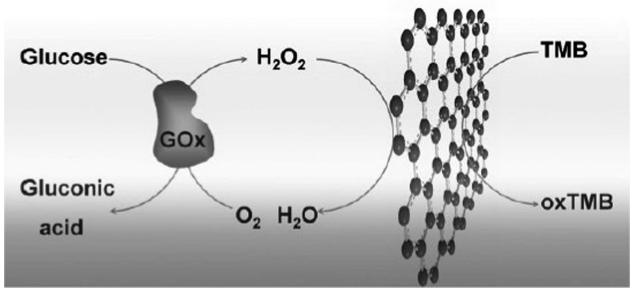

Fig. 2 Schematic illustration of colorimetric detection of glucose by using glucose oxidase and GO–COOH catalyzed reactions. Reprinted from ref. 36 with permission from Wiley.

functional groups on both the basal planes and edges.[25] Based on a series of detailed characterizations, Dekany's group have unraveled the chemical structure of GO and proposed a credible model, which has a corrugated carbon network including a ribbonlike arrangement of flat carbon hexagons connected by C=C double bonds (as seen in Fig. 1) and functional groups such as tertiary hydroxyl, 1,3-ether, ketone, quinine and phenol.[26,27] In addition, it has now been confirmed that epoxy and hydroxyl groups will reside on the GO basal surface, while carboxyl groups tend to attach to the edges of the GO plane.[28,29]

2.1.1. Catalytic oxidation reaction. Catalysis presents an important role in facilitating synthetically useful transformations. Very recently, Bielawski and Dreyer reported that GO could catalyze both the oxidation of alcohols and *cis*-stilbene, and the hydration of various alkynes under relatively mild conditions with excellent yields and desired selectivities.[12] This is the first example of graphene-based materials as metal-free catalysts in synthetic applications, opening up a new research field. To confirm the catalytic role of GO in the oxidation process, a series of control experiments were designed by the authors, and it was indicated that GO would undergo partial reduction during the catalytic conversion. The authors studied the recyclability of the GO catalyst, and no influence was observed on the activity of oxidation benzyl alcohol into benzaldehyde under high initial loadings ($\geq$50 wt%). However, the recovered GO catalyst exhibited only approximately 5% conversion at low catalyst loadings ($\leq$20 wt%). It was proposed that the reduced GO was converted to GO during the catalytic process under high catalyst loadings.

Bielawski and co-workers have made significant contributions to GO's catalytic applications[30] by using GO in a series of other catalytic reactions, including the oxidation of sulfides and thiols,[14] C–H oxidation,[31] Claisen–Schmidt condensation,[32] polymerization of various olefin monomers,[33] ring opening polymerization of various cyclic lactones and lactams,[34] and dehydration polymerization in the synthesis of carbon reinforced poly(phenylene methylene) composites.[35] Their contributions inspired a great deal of interest among the public, inspiring many groups to explore GO's catalytic performance in more catalytic reactions.

Qu and co-workers have developed a colorimetric method for glucose detection as illustrated in Fig. 2.[36] GO–COOH was prepared by adding NaOH and chloroacetic acid into GO solution to convert the –OH groups to –COOH *via* conjugation of acetic acid moieties.[37] Based on the catalytic performance of GO–COOH samples in the reaction of 3,3,5,5-tetramethylbenzidine oxidation in the presence of H_2O_2, GO–COOH has been demonstrated to possess intrinsic peroxidase-like activity to produce a blue color reaction following a ping-pong mechanism, with a maximum reaction rate of $(3.85 \pm 0.22) \times 10^{-8}$ M s^{-1}. This method was simple, cheap and highly selective, and was successfully employed for glucose detection in buffer solution, diluted blood and fruit juice. These findings facilitate GO's utilization in medical diagnostics and biotechnology.

Liu *et al.* have obtained GO foam *via* freeze drying, which was found to serve both as a reactant affording reduced GO and as a catalyst to convert SO_2 to SO_3.[38] Tan *et al.* reported the first example of using GO to facilitate the synthesis of organic compounds under visible light irradiation. GO was employed as a cooperative catalyst to rose Bengal, contributing to the photocatalytic oxidative C–H functionalization of tertiary amines to generate imines,[39] which have great value in the synthesis of many industrially important materials and biologically active compounds. Cao *et al.* reported the first convenient metal-free catalytic process for an efficient imine synthesis from various amines under mild and neat conditions with molecular oxygen as the terminal oxidant.[40] Based on the oxidative coupling of amines to imines, Su and co-workers have probed the activity of GO and studied its catalytic mechanism. Through the base and acid treatment of GO, it was found that the carboxylic groups as well as the localized unpaired electrons facilitated synergistic intermolecular arrangements, contributing to the enhanced catalytic activity of oxidative coupling of various primary amines.[29]

In order to understand the experimental results, theoretical simulations have also been employed to study the catalytic transition states and the oxidation process of GO catalysts. Bouklhvalov and co-workers have investigated the catalytic properties of GO based on the oxidation model of benzyl

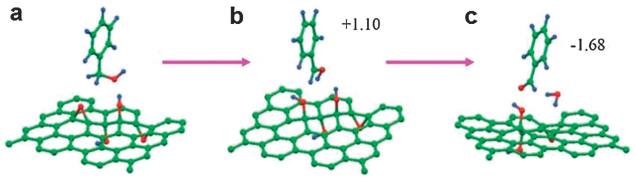

Fig. 3 Optimized atomic structures for the (a) initial, (b) intermediate and (c) final steps of benzyl alcohol oxidation over GO with the initial coverage of epoxy and hydroxyl groups, in which 12.5% of the carbon atoms are on the material's basal plane. The total energy costs of the reactions are reported in eV. From ref. 41 with permission from Wiley.

alcohol to benzaldehyde.[41] Based on density functional theory (DFT) calculations, it was revealed that the reaction proceeded *via* the transfer of hydrogen atoms from the organic molecule to the GO surface. The GO model with 12.5% of the carbon atoms covered by hydroxyl and epoxy groups has been established initially (as seen in Fig. 3). As the benzyl alcohol molecule moved close to the GO surface, one hydrogen atom would transfer from $PhCH_2OH$ to an epoxy group of GO, forming a diol on the GO sheet. The formation of dangling bonds on $PhCH_2OH$ or on GO was found to be energetically unfavorable, making this step endothermic. Then another hydrogen atom of benzyl alcohol molecule would migrate to one of the hydroxyl group on the GO surface, which resulted in the formation of one equivalent of water, and this step was exothermic. These simulated results have depicted detailed images of GO's catalytic process and were in agreement with the above-mentioned experimental results of Bielawski and Dreyer, where the radical groups were found to disappear after catalytic courses.[12]

2.1.2. Electrocatalysis. Electrocatalysis is one of the most important catalytic areas and GO possesses excellent activity toward many pivotal transformations. The electro-oxidation of ascorbic acid, uric acid, dopamine and acetaminophen using GO have been reported by Su's group.[42] They prepared the GO modified electrode by employing *in situ* electrochemical oxidation of graphite, as seen in Fig. 4. During the positive scans, the van der Waals force between graphitic sheets could be weakened owing to the oxidation process, and might be broken with the aid of gas evolution, forming few-layer GO sheets. Taking oxidation of ascorbic acid as an example here, the obtained low oxidation potential and high oxidation current demonstrated very good potential for electrochemical applications, which was explained by the increased surface area and oxygen functional groups of GO compared to graphite. Based on the high sensitivity and apparent peak separations for different analysts, it was proposed that GO-modified electrodes might find wide applications for biosensors and bioanalysis. Apart from this, reduced GO sheet films were also prepared by Li *et al.* as advanced electrode materials, and they have exhibited fast electron-transfer kinetics and possessed excellent electrocatalytic activity toward oxygen reduction.[25,43]

2.1.3. Photocatalysis. TiO_2 has been widely recognized as a good photocatalyst due to its suitable energy gap. GO is proved to be a semiconductor or an isolator while pristine graphene

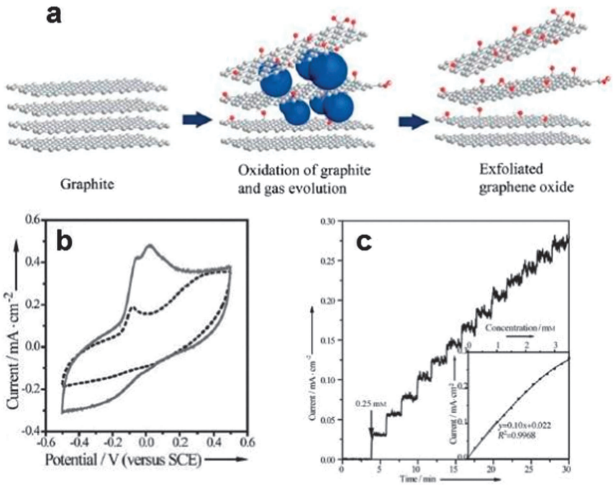

Fig. 4 (a) Schematic of the exfoliation process (gray, red, white and blue stand for carbon, oxygen, hydrogen and gas, respectively). (b) CV curves obtained from 3.0 mM ascorbic acid in 0.1 M PBS (pH = 6.9) with a scan rate of 20 mV s^{-1}; the dotted and solid lines stand for graphite and GO electrodes, respectively. (c) Amperometric response of GO-modified electrode held at 0.0 V for successive injection of ascorbic acid under constant magnetic stirring. Inset: calibration plot of current *vs.* ascorbic acid concentration. Adapted from ref. 42 with permission from Wiley.

has a zero band gap. Oxygenated components attached to the pristine graphene surface are tightly related to its band structure and the induced band gap opens up possibilities for photocatalytic applications. A GO semiconductor with an apparent band gap of 3.3–4.3 eV for direct transition and 2.4–3.0 eV for indirect transition was synthesized by Teng's group.[44] This band gap energy was sufficient to overcome the endothermic energy required for the water splitting reaction (1.23 eV). With the irradiation of both UV and visible light, abundant and continuous hydrogen evolution was obtained for reactions conducted in a 20 vol% aqueous methanol solution. The schematic corresponding energy-levels are displayed in Fig. 5. No noticeable degradation of GO was observed, demonstrating its high catalytic performance. Methanol was considered as a sacrificial hole scavenger, which could catch the photo-generated holes in the valence band of GO, avoiding electron–hole recombination.

In addition, Chen *et al.* reported an efficient photocatalytic conversion of CO_2 to methanol using GO as a catalyst,[45] and its schematic illustration is shown in Fig. 6. H_3PO_4 was used to react with hydroxyl groups forming esters, which could prevent the GO basal plane from further oxidation. GO with band gap in the range of 3.2–4.4 eV was obtained, which was sufficient to overcome the endothermic characteristics of the CO_2 reduction under solar energy excitation. The O containing chemical groups would stretch the band gap energy and help the electrons excite from the valence band to the conduction band, leading to photo-generated electrons and holes, which served as oxidizing and reducing radicals, respectively.

2.1.4. Other catalytic applications. Further efforts were devoted to the catalytic application of GO, since it was predicted that GO can be applied in other catalytic transformations

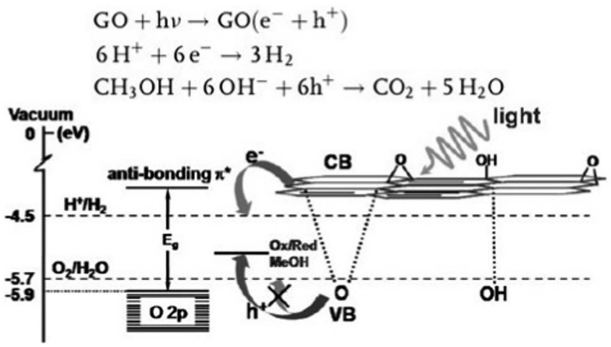

Fig. 5 Schematic energy-level diagram of GO relative to the levels for H_2 and O_2 generation from water. During photocatalytic reaction the conduction band of GO with a high overpotential relative to the level for H_2 generation exhibits fast electron injection from the excited GO into the solution phase, whereas the holes in the valence band of GO do not interact with the water molecules for O_2 generation, but are removed by the hole scavenger (methanol) instead. The possible mechanism for this methanol assisted water splitting is shown in the inset. Reproduced from ref. 44 with permission from Wiley.

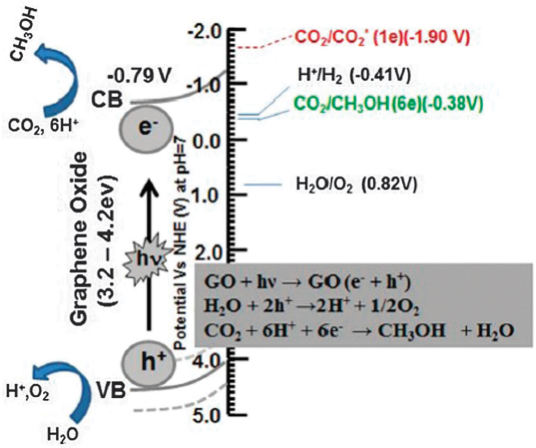

Fig. 6 Schematic illustration of the photocatalytic CO_2 reduction mechanism on GO, reproduced with permission from ref. 45, copyright 2013, Royal Society Chemistry.

due to its great chemical activity induced by the presence of plentiful oxygen-containing functional groups. For example, it has been shown to be an recyclable acid catalyst for ring opening reaction of epoxides with methanol or other primary alcohols as nucleophiles and solvents.[46] It has also been proved to be an efficient and reusable catalyst for the acetalization of aldehydes at room temperature,[47] aza-Michael addition of amines to activated alkenes,[48] Friedel–Crafts addition of indoles to α,β-unsaturated ketones,[49] synthesis of dipyrromethane and calyx[4]pyrrole[50] and oxidative dehydrogenation of propane.[51] All of the above results demonstrated the crucial role of the hetero oxygen element for the generation of active reactions sites on graphene sheets, which proves to be highly beneficial to its catalytic applications. Although GO is active in so many different transformations, its exact role in these catalytic processes needs more detailed investigations. Considering the complexity of the surface oxygen-containing groups, detailed characterizations are required to understand their distributions. Careful investigations on the differences of the mechanism in different reactions are much needed, which would also help to expand the applications of GO in other catalytic reactions.

2.2. N-doped graphene (χ = 3.04)

N-doped graphene (N-graphene) has been the most intensively studied doping model. N is next to C in the periodic table of chemical elements, and its electronegativity is larger than that of C (χ = 2.55). As such, the introduction of N into graphene sheets could modify its local electronic structures. The N heteroatom could be introduced directly during the graphene growth, by a CVD method using NH_3 and CH_4 as the N and C sources[52] or *via* a solvothermal process using lithium nitride and tetrachloromethane.[53] Alternatively, N can be doped through post treatment of graphene or GO, such as hydrazine reduction,[54] thermal annealing in ammonia,[55,56] and the arc-discharge method.[57] It has been well established that the incorporation of N atoms into the graphene matrix can lead to three main types of N formats, including graphitic N with direct substitution structure, and pyridinic N and pyrrolic N structures.[58] Graphitic N means the doping N atom is combined into a hexagonal ring. Pyridinic and pyrrolic N donate one and two p electrons to the π system, forming sp^2 and sp^3 hybridized bonds, respectively.[59] More interestingly, it was confirmed that N-doped carbon materials can improve their biocompatibility significantly.[60] It is expected that N-doped graphene will find more and more applications in the field of catalysis.

2.2.1. Oxygen reduction reaction. The fuel cell is an important electrochemical energy conversion device, which generates electricity from chemical energy directly through the reaction between a fuel and an oxidant in its electrodes.[61] The oxygen reduction reaction (ORR) at the cathode plays a key role in determining cell performance, cost and durability.[62] Currently, Pt based material is regarded as an active and efficient catalyst for ORR. However, many issues including the high cost, CO poisoning and agglomeration trend have hindered its commercialization.

N-graphene was reported for the first time to be a valuable catalyst for ORR by Dai's group in 2010.[63] Ni was employed as the catalyst and they developed a facile CVD approach with a N containing reaction gas mixture of $NH_3:CH_4:H_2:Ar$ at 10 : 50 : 65 : 200 standard cubic centimeters per minute for the synthesis of N-graphene films on a large scale. The N/C atomic ratio was *ca.* 4% for the obtained N-graphene and it was demonstrated to act as a superb metal-free electrode for ORR associated with alkaline fuel cells. As shown in Fig. 7, the pristine graphene electrode exhibited a two electron process for oxygen reduction with the onset potential of about −0.45 and −0.7 V. In contrast, the N-graphene electrode displayed a one step, four electron pathway, which is more efficient for ORR. Meanwhile, the steady catalytic current density of N-

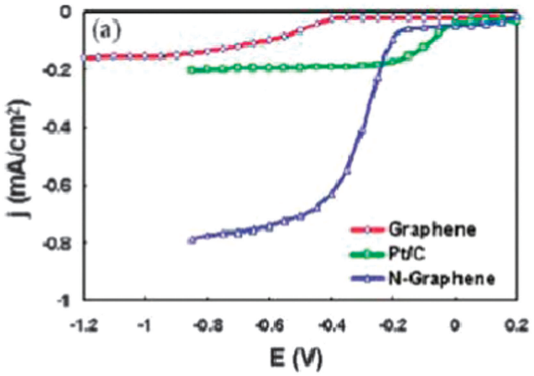

Fig. 7 The rotating ring disk electrode voltammograms for the ORR in air saturated 0.1 M KOH at the pristine graphene electrode (red line), Pt/C electrode (green line), and N-graphene electrode (blue line). Adapted from ref. 63 with permission, copyright 2010, American Chemical Society.

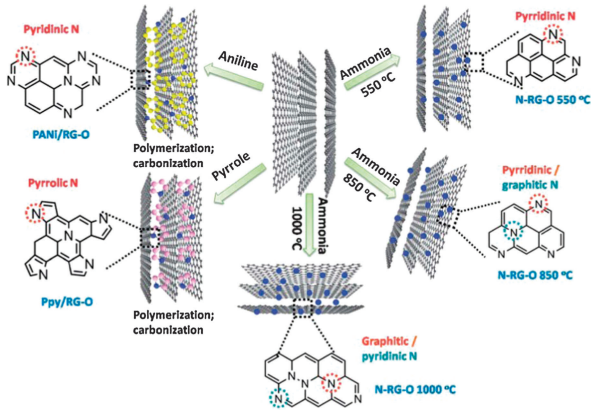

Fig. 8 Schematic diagram for the preparation of N-graphene with different N states. Reprinted with permission from ref. 65, copyright 2012, Royal Society Chemistry.

graphene is nearly 3 times higher than that of the commercial Pt/C electrode over a large potential range. In addition, N-graphene was insensitive to CO, resolving the severe drawback of Pt nanoparticles. This new metal-free catalyst showed high selectivity, long-term operation stability and fine tolerance to crossover effect, suggesting its great potential for other catalytic applications beyond fuel cells.

Sun and co-workers prepared N-graphene by heat treatment of graphene using ammonia, leading to 2.8 at% N doping at the optimized temperature of 900 °C.[64] The resultant N-graphene exhibited a very high ORR activity through a four electron transfer process in oxygen saturated 0.1 M KOH electrolyte, comparable or even better than commercial Pt/C (Pt loading: 4.85 μg cm^{-2}) electrodes. Based on the X-ray photoelectron spectroscopy (XPS) analysis, they attributed the enhanced ORR activity to the graphitic N atoms (substitutional doping) owing to the matching relationship between activity and graphitic N contents. Soon after, Ruoff *et al.* attributed this enhanced activity to pyridinic and pyrrolic N atoms, which was in conflict with Sun's result above. They obtained N-graphene with different N doping formats *via* annealing GO with different N sources,[65] and the schematic diagram is shown in Fig. 8. Through annealing of GO with ammonia, polyaniline or polypyrrole, the content of graphitic N species, pyridinic N centers and pyrrolic N moieties could be tuned, making this process more suitable for practical applications. Interestingly, the total atomic content of N in the metal-free N-graphene catalyst does not influence the ORR process under alkaline conditions. Instead, the activity of this novel catalyst was found to be dependent on the graphitic N content, which was related to the limiting current density. Moreover, the onset potential for ORR could be improved by the increasing pyridinic N content, which gradually converted the two electron pathway to a four electron process.

It is still very controversial as to whether the pyridinic N format or the graphitic N configuration determines the ORR activity. Moreover, whether the two-electron or four-electron pathway dominates is also under debate. Xia's group used high purity argon as a protective gas to anneal GO and melamine, and obtained highly doped N-graphene with up to 10.1 at% N.[66] Through the electrocatalytic measurement with 0.1 M KOH aqueous solution electrolyte, it was found that the activity of N-graphene toward ORR was higher than graphene and not considerably affected by the alteration of N content. As a result, it was concluded that the pyridine-like N component determined the electrocatalytic activity of N-graphene for ORR. Similar results were also given by Woo *et al.*[67] Hydrazine was used to deoxidize GO and their ORR activity in acid media was attributed to pyridinic N centers, higher than the commercial vulcan carbon.

In contrast, Lin and co-workers obtained pure pyridinic N atom doped single layer graphene with N percentage of up to 16 at% by the CVD method using hydrogen, ethylene and ammonia.[68] In the KOH electrolyte solution with pH = 13, the resultant two electron mechanism of ORR suggested pyridinic N might not be an effective promoter for ORR. On the other hand, a 3D porous structure of N-graphene with a high graphitic N doping level (~44 at%) has been obtained from polypyrrole, and it exhibited good activity for both ORR and oxygen evolution reactions (OER).[69]

Interestingly, Dong *et al.* synthesized N-graphene by a solvothermal method, and showed that N-graphene could act as a catalyst to facilitate four electron oxygen reductions in alkaline solution and two electron reduction in acidic solution.[59] The doped N atoms introduced electronic states around the Fermi level of graphene, helpful for the electron transfer from the band of graphene to anti-bonding orbitals of oxygen molecules, weakening the O–O bond and contributing to the reduction of oxygen molecules.[70]

To understand the catalytic mechanism for catalyst design and resolve these controversies, a series of simulation works have been carried out.[71,72] Boukhvalov and Son calculated the energetics of N-graphene catalyzed ORR with different amounts of N doping. It was found that a small amount of graphitic N doping decreased the energy costs at the intermediate steps of oxygen reduction significantly and the energy barriers were

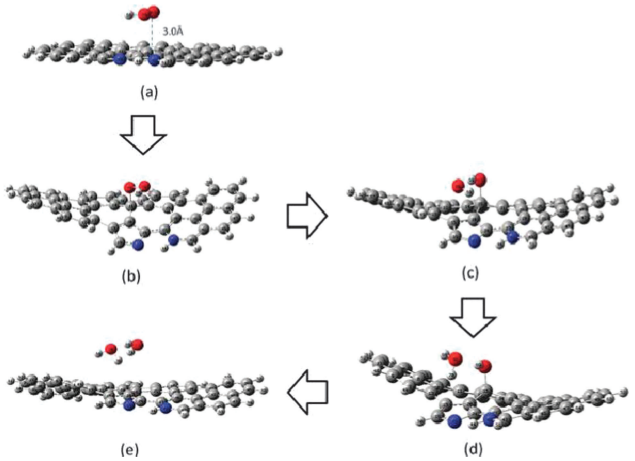

Fig. 9 Optimized structure of each electron transformation in ORR: (a) initial position of OOH from N-graphene, (b) OOH adsorbs on the doped graphene, (c) O–O bond is broken, (d) one water molecule is generated, and (e) C–O bond is broken, the second water molecule is generated. Gray, blue, red and small white balls represent C, N, O and H atoms, respectively. With permission from ref. 75, copyright 2012, American Chemical Society.

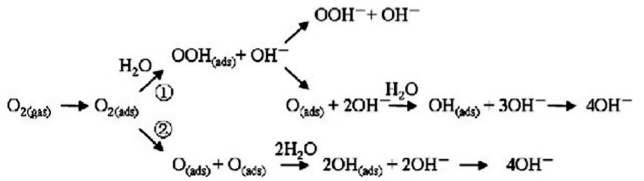

Fig. 10 Reaction scheme of ORR on N-graphene in alkaline solution, where ① presents an associative mechanism and ② a dissociative mechanism. Reproduced from ref. 79 with permission from Elsevier.

even lower than that on a Pt surface for the same process.[73] In contrast, Xia's group have simulated the ORR process on N-graphene with pyridinic doping in acidic fuel cells using B3LYP hybrid density functional theory.[74,75] The N doping could introduce high positive spin density and asymmetry atomic charge density, leading to a high catalytic activity. This electrocatalytic process could occur spontaneously on N-graphene as seen in Fig. 9, and the calculated average reversible potential was 1.15 V per SHE, which was consistent with the experimental results.

Based on the above results, it is still difficult to reach a unified conclusion because the graphitic and pyridinic N doping formats are only considered separately in the ORR process. This problem was partially addressed by Oshima *et al.*[76] They showed that catalysts with a relatively larger amount of graphitic N exhibit higher ORR activity than those with a relatively larger amount of pyridinic N atoms. Meanwhile, Ikeda's calculations suggested oxygen molecules are preferentially adsorbed associatively at C sits near the doped graphitic N moieties.[77] In addition, Anderson and co-workers showed there was no evidence for the direct four electron oxygen reduction to water over N-graphene with pyridinic edge sites,[71] suggesting that pyridinic N centers are a bad design for ORR applications. Very recently, Murakoshi *et al.* selectively doped pyridinic N and graphitic N within the graphene matrix with pyridine and julolidine as the N containing precursor molecules, and they proceeded *via* four- and two electron reduction pathways, respectively, in alkali-based solutions.[78] In addition, Bao *et al.* studied the surface coverage, electrode potential and solvent effect on the catalytic process based on the graphitic N-graphene model, aiming to understand the basic chemistry of ORR on N-graphene.[79] It was concluded from their results that: (1) hydrogen bonds of water would polarize oxygen molecules, facilitating their adsorption on N-graphene significantly; (2) associative mechanism and four electron reduction pathway were dominant in ORR; (3) the removal of adsorbed O from N-graphene surface was the rate determining step. Fig. 10 displays the possible reaction pathways obtained from their discussion. In order to unambiguously resolve this problem, samples with pure graphitic and pyridinic N doped single layer graphene should be prepared and compared in ORR measurements. Moreover, DFT simulations need to be carried out to support the experimental results.

2.2.2. C–H bond activation reaction. C–H bond activation is an important reaction traditionally catalyzed by transition metals and organometallic complexes.[80] Cheap metal-free catalysts have emerged as promising candidates for this transformation. N-graphene was reported to exhibit high activity and selectivity for the oxidation of arylalkanes in aqueous phase, affording high value-added products for biomedical applications.[81] The N-doped sp^2 hybridized carbon was prepared through a CVD process with acetonitrile vapor as the N source with 8.9% N content. Control experiments on different carbon materials suggested the N doping greatly enhanced catalytic activity as well as selectivity, and the activity was not related to the surface area of the catalysts.

DFT simulation was carried out to study the catalytic mechanism with graphitic N as the doping format according to the XPS result. Interestingly, the catalytic active site was the *ortho* carbon site, as shown in Fig. 11a, instead of the doped graphitic N. Based on electronic partial density calculations, it was indicated that the density states near the Fermi level for *ortho* carbon are higher than those of other nearby C atoms, conferring it a metal-like d band electronic structure and a more metal-like catalytic performance.

2.2.3. Reduction of nitro compounds. Nitro compounds are prevalent organic pollutants generated from agricultural and industrial sources.[82] Meanwhile, the conversion from nitro to amino groups has great industrial relevance, such as for preparing aniline and paracetamol.[83] The reduction of 4-nitrophenol (Nip) to 4-aminophenol (Amp) by sodium borohydride (BH_4^-) was found by Pal *et al.* in 2002[84] and it has become almost the most often used reaction to test the catalytic activity of catalysts in aqueous solution.[85] Almost all of the existing investigations on this reaction were based on metallic material under mild conditions. Recently, our group reported the synthesis of N-graphene by hydrothermal treatment of GO and

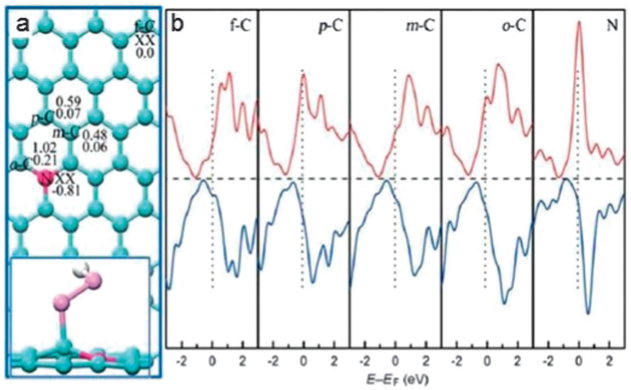

Fig. 11 (a) Schematic representation of different catalytic sites for peroxide adsorption on the N-graphene. The adsorption energy is listed in the top line (in eV) beside the corresponding sites; "XX" indicates that peroxide can not be adsorbed on the site. The charge of different sites before formation of peroxide is shown in the second line (in a). The inset at the bottom of (a) shows the local configuration of peroxide on *ortho* carbon site of N-graphene. (b) The electronic partial density of states for N and C in different positions of N-graphene. Reproduced from ref. 81 with permission from Wiley.

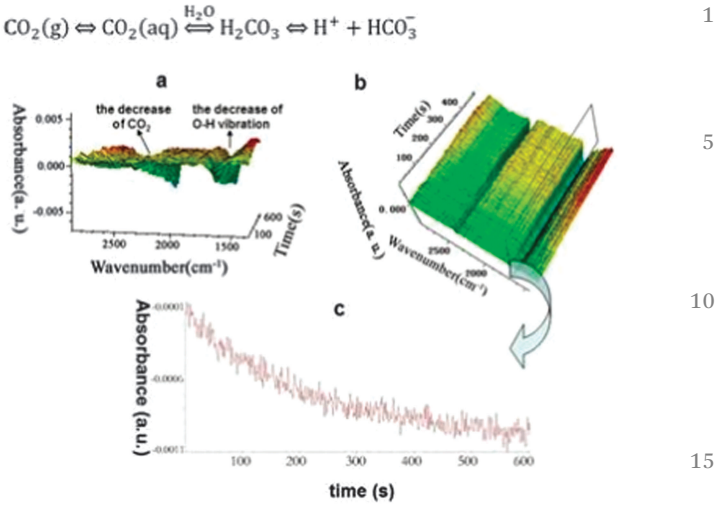

Fig. 13 *In situ* FTIR of the mixture composed of Nip and NG lonely (a) in side view and (b) in top view; (c) the absorbance variation of O–H vibration with time. With permission from ref. 86, copyright 2013, Royal Society Chemistry.

ammonia, and its catalytic behavior in the reduction of Nip to Amp.[86] Interestingly, the N-graphene catalytic process was found to follow zero order kinetics (as seen in Fig. 12), which was different from the first order kinetics observed using all of the traditional metallic catalysts.

This result demonstrated the difference between N-graphene and metallic catalysts, and it could be explained by the smaller active sites. DFT calculations have also been employed to simulate the adsorption configuration of Nip ion on this metal-free catalyst according to the XPS and *in situ* FTIR results (as seen in Fig. 13). Only the carbon atom near the doped N atom could be activated to catch Nip ions owing to its weaker conjugation compared to other carbon atoms, so the number of active sites on the graphene surface was much smaller than those of metallic nanoparticles. Therefore, the adsorption process of Nip ions on the surface of N-graphene was more pivotal than in the cases of metals, changing its reaction kinetics. Furthermore, the active sites of N-graphene were positively charged owing to the large electronegativity of doped N atoms, so Nip ions preferred to combine with graphene sheet *via* the atom of hydroxyl group, as based on the Mulliken analysis it had a charge of −0.450 electrons, more negatively charged than the −0.246 electrons of the nitro group. This was in agreement with the decrease of O–H vibration of the *in situ* FTIR results.

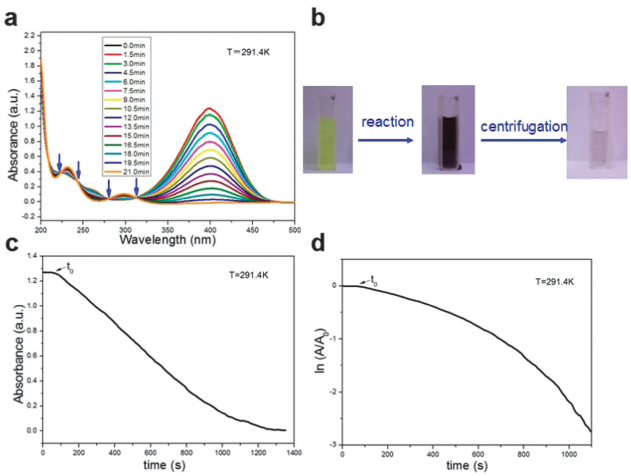

Fig. 12 (a) Typical absorption spectra of Nip by BH_4^- as the catalytic reaction proceeded, where the molar ratio between Nip and $NaBH_4$ was selected as 1 : 100; (b) photos of the color change during the catalytic reaction for NG. (c) and (d) Time curves of the absorbance measured for the NG catalyst, indicating zero order kinetics. Reprinted with permission from ref. 86, copyright 2013, Royal Society Chemistry.

In addition, Xia and co-workers reported the enhanced electrocatalytic activity toward the reduction of nitroaromatic compounds with a decreased overpotential compared with thermally reduced graphene.[87] Four nitro compounds – 2,4,6-trinitrotoluene, 1,3,5-trinitrobenzenein, 2,4-dinitrotoluene and 1,3-dinitrobenzene – were tested using N-graphene. The onset and peak potentials both shifted positively on N-graphene compared to the thermally reduced graphene, indicating a greatly decreased overpotential and the excellent activity of this new metal-free catalyst.

2.2.4. Oxidation of benzylic alcohols. Recently, Wang's group have employed a heat treatment procedure to synthesize N-graphene and reported its efficient catalytic activity toward aerobic selective oxidation of benzylic alcohols.[88] It was found that the nitridation temperature greatly influenced the N doping concentrations and formats. Graphitic sp^2 N atoms were found to be the active sites with good linear correlation with activities (as seen in Fig. 14(a)). The activation energy and pre-exponential factor were 56.1 ± 3.5 kJ mol^{-1} and 2.32 × 10^3, respectively, following a Langmuir–Hinshelwood kinetic pathway. The reaction process was proposed based on electron

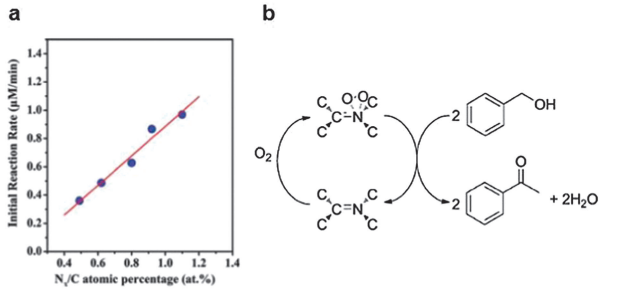

Fig. 14 (a) Relationship between initial reaction rate and graphitic N species; (b) the proposed reaction pathway for the aerobic alcohol oxidation over N-graphene. With permission from ref. 88, copyright 2012, American Chemical Society.

paramagnetic resonance characterization (shown in Fig. 14(b)) and it is suggested that the formation of the intermediate product of sp^2 N–O_2 had a high chemical reactivity towards alcohols.

2.2.5. Electrochemical biosensing. Glucose oxidation is of great significance in life sciences. As N-graphene has good biocompatibility and has been demonstrated to be a highly efficient catalyst, its application in biosensing was investigated. Lin *et al.* used N plasma treatment to produce N-graphene, and the N content could be tuned from 0.11 to 1.35% by controlling the exposure time.[89] N-graphene had good response and high sensitivity toward glucose oxidation, exhibiting fast electron transfer kinetics. As shown in Fig. 15, the influence of ascorbic acid and uric acid has also been studied, and glucose with concentrations as low as 0.01 mM could be detected by N-graphene, indicating its potential applications in biosensing.

Reduction of hydrogen peroxide by N-graphene has also been investigated,[90,91] and the obtained excellent electrocatalytic activity suggested its potential applications in measuring H_2O_2 release in living cells.[91] In addition, calculations indicated that the reactivity had the following order: pyridinic N-graphene > pyrrolic N-graphene > graphitic N-graphene > pristine graphene, which could be explained by the calculated electrostatic potential distributions.[92]

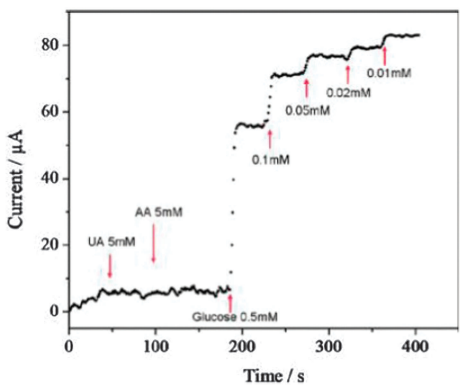

Fig. 15 Chronoamperometric responses to successive addition of 5 mM uric acid (UA), 5 mM ascorbic acid (AA), 0.5 mM glucose, 0.02 mM glucose, and 0.01 mM glucose on N-graphene electrode immobilized with glucose oxidase at −0.15 V in 0.1 M PBS (pH 7.0). From ref. 89, copyright 2010, American Chemical Society.

Due to the great performance of N-graphene in electrocatalytic reactions, it has been applied as a sensor for simultaneously determining small biomolecules including ascorbic acid, dopamine and uric acid.[93] Moreover, it was found that this metal-free catalyst could reduce triiodide by replacing the Pt cathode in dye sensitized solar cells, resulting in a power conversion efficiency of up to 7.07%.[94] In general, N-graphene has shown many superior features in metal-free catalysis including high efficiency, high stability, recyclability, biocompatibility, making it highly attractive for further investigations.

2.3. B-, S-, P-, Se-, I- and Si-doped graphene and H-decorated graphene

2.3.1. B-doped graphene (χ = 2.04). B element has unique and basically incomparable properties. Investigations on B-doped graphene (B-graphene) have also been carried out,[95,96] since B and N both are next to C in the periodic table of chemical elements. B-graphene could be synthesized *via* thermal annealing of graphite oxide in the presence of boron oxide as the B source.[97] Although the electronegativity of B is smaller than that of N, B-graphene also showed excellent activity toward ORR in alkaline electrolytes. Furthermore, it exhibited long-term stability and fine CO tolerance, which was superior to Pt-based catalysts. Recently, our group carried out DFT calculations, which suggest B doping could induce local high spin density on the basal plane owing to its strong electron withdrawing capability, which plays a key role in facilitating the adsorption of oxygen and OOH molecules and enhances the ORR compared with pristine graphene.[98] As shown in Fig. 16, as the doped B atom had only three valence electrons, its p_z orbital should be vacant, leaving an unpaired single p_z electron on the neighboring C atom, which induced an interesting local spin density. Meanwhile, since the electronegativity of B was smaller than that of C, the paired covalent electrons will be slightly polarized towards the C atoms, forming local positive charge density on the B atoms as depicted in Fig. 16b, which could be taken as new active sites for catalysis. Furthermore, the simulated ORR process demonstrated that the OOH cluster

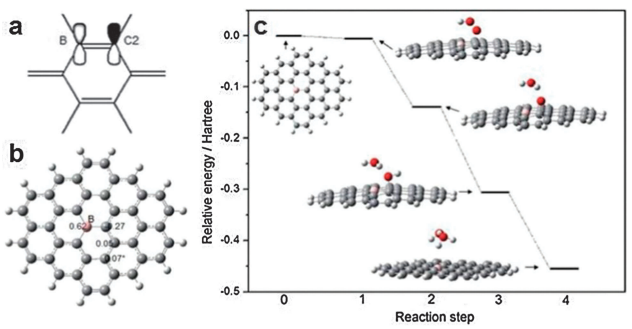

Fig. 16 (a) The source of the high spin density for B-graphene, (b) the calculated NBO charge density distribution in unit of a.u. for B-graphene, (c) relative energies of the reaction pathways of ORR on B-graphene. Reproduced from ref. 98 with permission from Wiley.

could adsorb on B-graphene tightly and this whole catalytic reaction was an exothermal process with no energy barrier, eventually forming two water molecules.

2.3.2. S-doped graphene (χ = 2.58). The electronic structure of S-doped graphene (S-graphene) was investigated by simulations, which revealed that it could be either a semiconductor with a small band gap or a metallic form, depending on the content of doped sulfur.[99] Experimentally, both hydrogen sulfide[100] and benzyl disulfide[101] have been used as S sources, leading to S-graphene formation from GO. Mullen *et al.* indicated that S could be introduced into graphene sheets in a major form of thiophene-like S.[100] In both cases, good catalytic activities in ORR were observed, demonstrating S-graphene as an excellent metal-free catalyst with high stability and selectivity. Furthermore, edge-selectively sulfurized graphene nanoplatelets have been produced by simple dry ball-milling graphite in the presence of sulfur (S_8) in 2013.[102] The schematic presentation is displayed in Fig. 17 and the obtained material shows good performance in ORR and its catalytic efficiency could be improved with further oxidation. Combined with theoretical analysis, the electronic spin density was found to be critical in the catalysis, with S atoms and O=S=O doped at the edges of graphene strongly promoting the electrocatalytic activity.

In another report, sulfated graphene, through acid treatment of graphene, has been prepared as an efficient solid catalyst. Quantitative energy dispersive X-ray spectroscopy (EDS) mapping showed element S was distributed on the whole surface of graphene homogeneously (Fig. 18).[103] Catalytic tests demonstrated the sulfated graphene was a good water tolerant catalyst with high activity for the hydrolysis of ethyl acetate,[103] dehydration of xylose[104] and acid catalyzed liquid reactions such as the esterification of acetic acid.[105]

2.3.3. P-doped graphene (χ = 2.19). P element is in the nitrogen group, and it has the same number of valence electrons as nitrogen and similar chemical properties. A thermal annealing approach has been used to fabricate P-doped graphene (P-graphene) with triphenylphosphine as the P source, and the obtained sample exhibited outstanding ORR activity (higher than graphene) as well as excellent selectivity and stability.[106] Very recently, Primo and García have prepared P-graphene by simple pyrolysis of alginate and $H_2PO_4^-$ in the absence of oxygen, and the obtained sample was shown to be a good photocatalyst for hydrogen generation from water–methanol mixtures. Moreover, it was found that an increase in the amount of HPO_4^{2-} increased its catalytic activity.[107] In addition, the existing calculations showed that P substitutional defect on graphene had low formation energy and would introduce a larger band gap energy.[108] Experimentally, triphenylphosphine has been used as P source to obtain P-doped graphite, which has showed high electrocatalytic activity, long-term stability, and excellent tolerance to crossover effects of methanol in ORR in an alkaline medium.[109]

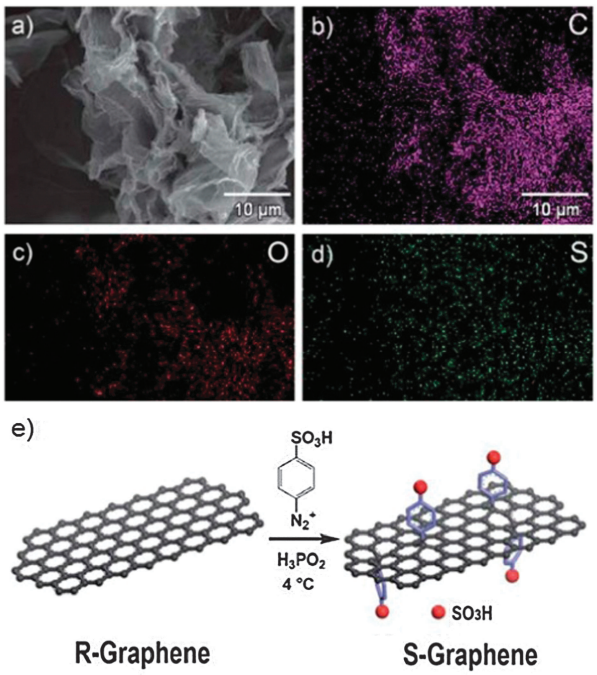

Fig. 18 (a) SEM image of the prepared sulfonated graphene, and corresponding quantitative EDS element mapping of (b) C, (c) O and (d) S. (e) Illustration for the preparation of sulfonated graphene. Reprinted with permission from ref. 103, copyright 2011, Royal Society Chemistry.

2.3.4. Se-doped graphene (χ = 2.55). Diphenyl diselenide protected by argon was selected as the Se source to introduce Se doping.[101,110] Se-graphene exhibited better catalytic activity for ORR than the commercial Pt/C in alkaline electrolyte, revealing good potential as a substitute for Pt-based catalysts in fuel cells.[101] It was shown that the ORR activity of an only 1 wt% Se-doped carbon material was comparable to N-doped carbon materials with 4–8 wt% of N, indicating the good performance of Se-graphene.[110] As the electronegativity of Se is the same as C atom, the induced charge redistribution should be smaller than for other foreign atom doping. Therefore, its good catalytic properties were explained by the large atomic size of Se, which would induce high strain at the edges of carbon materials, facilitating charge localization and contributing to oxygen adsorption. Moreover, the polarizability of Se was high and it was noted that lone Se pairs could easily interact with the surrounding molecules.

2.3.5. I-doped graphene (χ = 2.66). Iodine was deemed to be a p-type doping of graphene. Huang *et al.* prepared I-doped graphene (I-graphene) *via* annealing GO and I_2 at high temperature in argon.[111] The I-doping content could be controlled through adjusting the ratio of GO to I. The obtained I-graphene

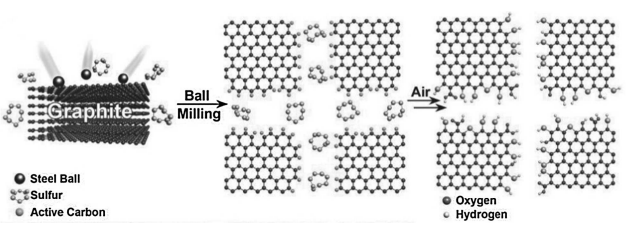

Fig. 17 A schematic representation of the ball-milling process. From ref. 102 with permission from Wiley.

displayed excellent catalytic activity, good reusability and high resistance to crossover effects for ORR. Based on XPS characterization and detailed analysis, it was confirmed that the formed I_3^- could induce a relatively higher positive charge density on the graphene surface, facilitating the reduction of oxygen to OH^-.

2.3.6. Si-doped graphene (χ = 1.90). Si doping in graphene is still rare and represents an emerging field, especially in catalytic research. To the best of our knowledge, there is no experimental report on catalysis using Si-doped graphene (Si-graphene). Zhao *et al.* investigated the adsorption of NO, NO_2 and N_2O on Si-graphene using DFT calculations, and found it could be an ideal sensor for NO and NO_2 detection.[112] Interestingly, when the greenhouse gas N_2O was adsorbed on Si-graphene in the [2+2]-cycloaddition configuration, a N_2 molecule was able to escape and leave an O atom attached to the basal plane with the O–Si bond of 1.581 Å, indicating that Si-graphene could be used as metal-free catalyst for N_2O reduction.

2.3.7. H-decorated graphene (χ = 2.20). H decoration is another important functional method to modify graphene. The fully hydrogenated graphene has been named graphane, and has every C atom combined with one H atom and all of the attached H atoms distributed on both sides of the basal plane, alternately. As it has not yet been fabricated, partial H-decorated graphene (H-graphene) may be more relevant in practice application. The hydrogenated methods include CVD fabrication and solution based reduction of graphite, as well as hydrogenation of sp^2 carbon materials in a hydrogen gas/plasma atmosphere.[19] Yan's group prepared H-graphene with the H/C ratio of 0.54 and reported its catalytic activity to be higher than the reduced graphene for the Fenton-like reaction to degrade organic dyes.[113] In addition, our group have found that H decoration could enhance the ORR performance of graphene based on DFT investigations.[98] The π covalent bond was broken due to H adsorption, forming single electrons and high local spin density, which was beneficial for oxygenated component adsorption, contributing to the ORR process.

Based on the above discussions, it can be concluded that two alterations in the surface structure contribute to the catalytic origins of the doped graphene: one is from the local high electron/spin density induced by the electronegativity difference of the doped element or the broken π covalent bonds caused by H decoration, the other is modifications at the edge of the graphene sheets, such as the induced high strain of Se and O═S═O groups doped by S. Both alterations in the surface structure facilitate the adsorption of reactants and improve the chemical activity. As such, it can be expected that new metal-free catalysts could be prepared by doping with other elements.

2.4. Graphene doped with two elements

With the development of doping technology, the growth of graphene co-doped with two elements has been explored by scientists. Co-doping using elements with different electronegativity could create a unique electronic structure and might bring in special synergistic effects. The electronegativities of B and N are 2.04 and 3.4, which are lower and higher than that of C element (χ = 2.55), respectively. B and N co-doped graphene (BN-graphene) has been used as a high performance solid state supercapacitor[114] and was predicted to be a good catalyst for the cathode ORR *via* first principles calculations.[115,116] Recently, it was fabricated through thermal annealing of GO in the presence of boric acid and ammonia by Dai *et al.*, showing superior electrocatalytic activities toward ORR in alkaline media, better than the Pt/C electrode.[117] The doping level could be adjusted, which directly influences the energy band gap, local spin density and charge distribution. Co-doping with two appropriate elements could create a new and smaller band gap that will increase the conductivity; calculations suggested $B_{12}C_{77}N_{11}H_{26}$ structure had the lowest energy gap, resulting in the highest chemical reactivity or the best catalytic performance.

In addition, Qiao and co-workers have investigated the catalytic performance of BN-graphene both experimentally and theoretically.[118] They prepared BN-graphene using a two step doping method, incorporating heteroatoms at desired sites on the graphene surface and preventing the formation of inactive by-products. For comparison, hexagonal boron nitride (h-BN) and B-graphene and N-graphene were selected to study the synergistic effect of the double doping. Fig. 19(a) shows a higher cathode current and a higher potential for BN-graphene, indicating a more efficient and more facile ORR process on the co-doped graphene. The transferred electron number in an ORR process was 3.97 for BN-graphene, higher than that of single doped graphene and h-BN, indicating excellent activity and perfect selectivity (four electron dominating pathway) for BN-graphene (as seen in Fig. 19(b)). The DFT

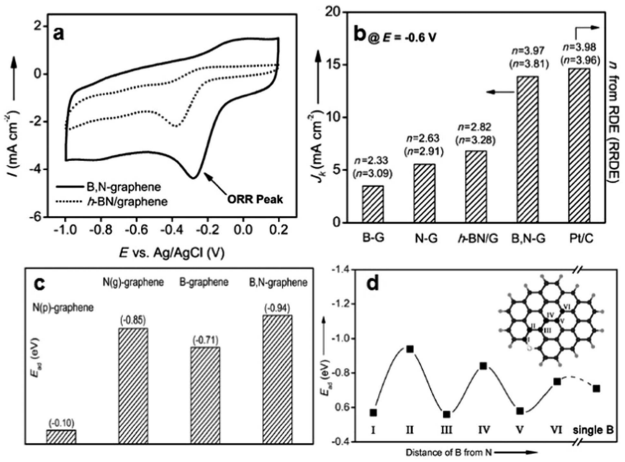

Fig. 19 (a) Cyclic voltammograms of ORR on BN-graphene and the h-BN–graphene hybrid in an oxygen saturated 0.1 M solution of KOH with a scan rate of 100 mV s^{-1}. (b) Summary of the kinetic limiting current density and the transferred electron number on the basis of the RDE data and the RRDE data (values in parentheses) on various catalysts. (c) Calculated adsorption energies of HO_2 for all of the selected catalysts. N(p) and N(g) indicate pyridinic and graphitic N bonding, respectively. (d) Adsorption energies on various BN-graphene with B active sites as a function of the distance to a pyridinic N atom. Reproduced from ref. 118 with permission from Wiley.

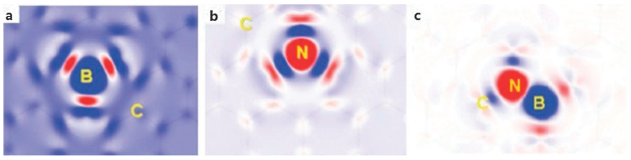

Fig. 20 The 2D charge redistribution in the graphene planar region calculated by the charge difference between the doped graphene and pristine graphene (blue for charge depletion and red for charge accumulation) of B-graphene, N-graphene and BN-graphene. With permission from ref. 119, copyright 2013, Royal Society Chemistry.

investigations revealed this co-doped sample had the largest combined energy for the adsorption of surrounding oxygen containing molecules. An alternative enhanced mechanism has been pointed out, as displayed in Fig. 19(d): a B atom *meta* to the doped N atom exhibited the highest adsorption energy, whereas an *ortho* B bonded directly to the N atom showed the lowest activity.

Another simulated investigation about the catalytic activity of BN-graphene has been completed by Fan *et al.*[119] They have systematically studied the ORR performance of BN-graphene, B-graphene and N-graphene. It was found that the charge redistribution happens mostly in the region of BN cluster with its nearest carbon atoms as shown in Fig. 20, and the formation of the epoxide group should be important for the four-electron process of BN-graphene.

In addition to BN-graphene, the authors have also fabricated S and N dual-doped graphene (SN-graphene).[120] Commercial silicon dioxide was used to create mesopores as seen in Fig. 21(a). The obtained SN-graphene exhibited good long term stability and high catalytic activity including very high kinetic limiting current and positive onset potential for ORR, indicating it would be a very suitable catalyst for the next generation of fuel cells. The great synergistic effect could be attributed to the redistribution of spin and charge densities induced by the co-doped S and N atoms, which was calculated as shown in Fig. 21(b).

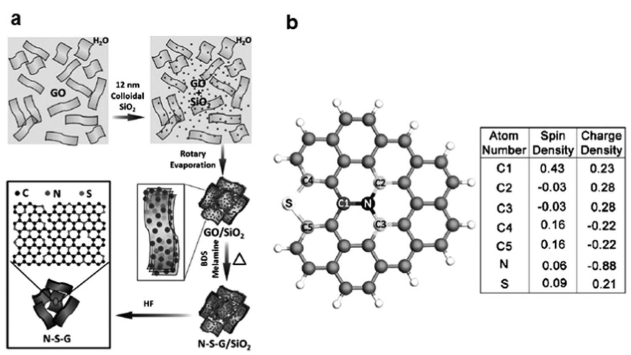

Fig. 21 (a) A schematic illustration of the fabrication of N and S dual-doped mesoporous graphene from GO. (b) Spin and charge density of graphene network (gray) dual-doped by N (black) and S (white). Reprinted from ref. 120 with permission from Wiley.

The S and N dual-doped graphene has also shown increased ORR activity in NaOH electrolyte with thiophene and pyrimidine as the precursors.[121] However, all of these mentioned promising co-doped catalysts were studied in alkaline media. Recently, Woo *et al.* have tried to use boric acid and phosphoric acid to introduce B and P to N-graphene, obtaining BN-graphene and P and N dual-doped graphene (PN-graphene), respectively.[122] Their ORR activities were studied in acidic media and both of them showed good performance, especially the PN-graphene. Its onset potential and mass activity were 0.87 V and 0.80 mA mg^{-1}, better than 0.75 V and 0.45 mA mg^{-1} of the original N-graphene, indicating a synergetic increased catalytic property due to the co-doping. The enhanced performance was attributed to the asymmetry enhancement of spin density caused by the dual-doped heteroatoms, as well as the induced facile electron transfer on the graphene basal plane and decrement of energy gap. The synergetic effect induced from double doping has further enhanced the catalytic performance of graphene, which also opens up more possibilities for the fine tuning of the properties of graphene-based materials. Currently, the studies of the co-doping effect are very preliminary. For example, extensive investigations are need to understand the exact formats and concentrations of the co-doped elements on the surface of the graphene, as well as their influence for the catalytic properties.

3. Conclusion and perspectives

Table 1 summarizes different reactions catalyzed by doped graphene. With the selection of appropriate precursors, different metal-free heteroatoms can be doped into graphene sheets, modifying its geometrical and electronic structures and inducing interesting active sites, which contribute to their different catalytic performance. The most common preparation method for GO is the Hummers method, which uses a strong oxidizing agent. GO has been widely studied and applied in many important catalytic reactions, especially for a series of oxidation reactions, in which the attached oxygenated groups on the graphene surface are pivotal as the active sites. For other heteroatom-doped graphene, such as N and B doping, there are two preparation methods in general: the first is the synchronous doping method, which depends on CVD technology, with the addition of an appropriate carbon source and heteroatom precursor, and the foreign element can be introduced into the graphene sheets during its growing process. The other method is the post treatment process, in which GO or reduced GO was prepared at first as graphene substrates, which are plasma treated or annealed at high temperatures with the introduction of heteroatom containing molecules, affording different doped graphene catalysts. In light of all these methods, it is still very difficult to control the doping concentration, doping and bonding formats, distributional uniformity as well as some other features. This is especially true for the co-doping cases. All of these features directly or indirectly determine the properties of the doped graphene in catalytic reactions.

Table 1 Summary of the doped graphene as metal-free catalysts. [*T*]: conversion rate; [*Y*]: yield; [*B*]: reaction barrier; [*V*]: maximum reaction rate

Doped graphene	Catalyst preparation	Doped level (atomic ratio)	Catalytic application	Catalytic efficiency	Ref.
GO	Hummers method	33.9%	Oxidation of benzyl alcohol	1.6×10^{-2} mol g^{-1} [*T*]	12
GO	Hummers method	35.5%	Oxidation of sulfides and thiols	Sulfides: 51–96% [*Y*] Thiols: 75–100% [*Y*]	14
GO	Hummers method	—	Oxidation of C–H	4–85% [*Y*]	31
GO	Hummers method	23.6%	Oxidation of glucose	$(3.85 \pm 0.22) \times 10^{-8}$ M s^{-1} [*V*]	36
GO	Hummers method	25.5%	Oxidation of SO_2	6.12 g g^{-1} [*T*]	38
GO	Hummers method	—	Oxidative C–H functionalisation of tertiary amines	90–97% [*Y*]	39
GO	Hummers method	—	Oxidative coupling of amines to imines	75–98% [*Y*]	29, 40
GO	Simulations	75% and 12.5%	Oxidation of benzyl alcohol to benzaldehyde	1.64 eV for 75% [*B*] 1.10 eV for 12.5% [*B*]	41
GO	*In situ* electrochemical oxidation of graphite	22.5%	Oxidation of ascorbic acid	—	42
GO	Hummers method	—	ORR	> Bare GC electrode	43
GO	Hummers method	30%	Generation hydrogen from water	> Pt/GO	44
GO	Hummers method	—	Conversion of CO_2 to methanol	0.172 μmol g cat^{-1} h^{-1}	45
GO	Hummers method	—	Ring opening of epoxides	7–99% [*T*]	46
GO	Hummers method	43.6%	Acetalization of aldehydes	2–95% [*Y*]	47
GO	Hummers method	—	Aza–Michael addition of amines to activated alkenes	65–97% [*Y*]	48
GO	Hummers method		Friedel–Crafts addition of indoles to α,β-unsaturated ketones	40–92% [*Y*]	49
GO	Hummers method	—	Synthesis of dipyrromethane and calyx[4]pyrrole	86–100% [*T*]	50
GO	Simulations	—	Oxidative dehydrogenation of propane	9.2–25.3 eV [*B*]	51
GO	Hummers method	—	Claisen–Schmidt coupling of methyl ketones and aldehydes	10–85% [*Y*]	32
GO	Hummers method	38.5%	Polymerization of various olefin monomers	100% [*T*]	33
GO	Hummers method	36.1%	Ring opening polymerization of various cyclic lactones and lactams	39–100% [*Y*]	34
GO	Hummers method	32.9%	Dehydrative polymerization	—	35
N-graphene	CVD method with CH_4 and NH_3 as C and N sources	4%	ORR	> Pt/C	63
N-graphene	Annealing graphene or GO with different N precursors	2.8%,[64] 5.5%,[65] 6.6%,[65] 7.36%,[65] 10.1%[66]	ORR	> Pt/C[64] > Pt & GC electrode[65] > Graphene[66]	64–66
N-graphene	Reducing GO by hydrazine	The ratio of C to N at the surface is 0.047	ORR	> Vulcan carbon	67
N-graphene	CVD method with ethylene and ammonia as C and N sources	16%	ORR	< Pt	68
N-graphene	Pyrolyzing the GO-polypyrrole composite	44%	ORR and OER	> Pt/C & graphene	69
N-graphene	Solvothermal method	10.5%	ORR	—	59
N-graphene	Simulations	4%,[73] 2.2%[74]	ORR	> Graphene	71, 73–75, 79
N-graphene	CVD method with pyridine and julolidine as N sources	2.7% pyridine	ORR	> Graphene	78
N-graphene	CVD method with acetonitrile vapor as the N source	2.0% julolidine 8.9%	Activating C–H bonds	91.3% [*Y*]	81
N-graphene	Hydrothermal treating GO with ammonia	11.1%	Reduction of 4-nitrophenol to 4-aminophenol	100% [*Y*]	86
N-graphene	Annealing GO with melamine	10.1%	Reduction of nitro explosives	> Thermally reduced graphene	87
N-graphene	Heating GO with NH_3	4.2%	Oxidation of benzylic alcohols	Activation energy: (56.1 ± 3.5) kJ mol^{-1}, close to 51.4 kJ mol^{-1} of Ru/Al_2O_3	88
N-graphene	N plasma treatment method	From 0.11% to 1.35%	Oxidation of glucose	> Graphene & GC electrode	89
N-graphene	N plasma treatment method	8.5%	Reduction of H_2O_2	> Pt	90
N-graphene	Simulations	2.2%	Reduction of H_2O_2	> Graphene	92

Table 1 (*continued*)

Doped graphene	Catalyst preparation	Doped level (atomic ratio)	Catalytic application	Catalytic efficiency	Ref.
N-graphene	Annealing GO with melamine	8.4%	Electrochemical determination of ascorbic acid, dopamine and uric acid	> Bare GC electrode	93
N-graphene	Annealing GO in ammonia	7.6%	Reducing triiodide	> Pt	94
B-graphene	Annealing GO in B_2O_3 vapor	3.2%	ORR	≈ Pt	97
B-graphene	Simulations	2.2%	ORR	> Graphene	98
S-graphene	Thermal treating of GO with H_2S	From 1.2% to 1.7%	ORR	> Pt/C	100
S-graphene	Annealing GO with benzyl disulfide	From 1.3% to 1.5%	ORR	> Pt/C	101
S-graphene	Ball-milling graphite in S_8	4.94%	ORR	> Pt/C	102
S-graphene	Sulfonated treatment of graphene	6.4%,[103] 1.8%[104]	Hydrolysis of ethyl acetate,[103] dehydration of xylose,[104] esterification of acetic acid[105]	> Nafion NR50[103] 61% [Y][104] > Mesoporous carbon & GO & SBA-15[105]	103–105
P-graphene	Annealing GO with triphenylphosphine	1.3%	ORR	> Graphene	106
P-graphene	Pyrolysis of alginate and $H_2PO_4^-$	7.3%	Hydrogen generation	> GO	107
Se-graphene	annealing GO with diphenyl diselenide	1.1 wt%[110]	ORR	> Pt/C[101] & graphene[110]	101, 110
I-graphene	Annealing GO with I_2	1.2%	ORR	> Pt/C & graphene	111
Si-graphene	Simulations	—	N_2O reduction	—	112
H-graphene	Gamma ray irradiation of GO	54%	Fenton like reaction to degrade organic dye	> Reduced graphene	113
H-graphene	Simulations	2.2%	ORR	> Graphene	98
BN-graphene	Simulations	—	ORR		115, 116, 119
BN-graphene	Annealing GO with boric acid and ammonia	—	ORR	> Pt/C	117
BN-graphene	Annealing GO with NH_3 for N doping, and then pyrolysing the intermediate with H_3BO_3	—	ORR	> B-graphene & N-graphene & h-BN/graphene	118
BN-graphene	Pyrolysis of graphene-dicyandiamide for N doping, and then pyrolysing it with boric acid	—	ORR	> N-graphene	122
SN-graphene	Heating GO with melamine and benzyl disulfide	—	ORR	> N-graphene & S-graphene	120
SN-graphene	CVD method with benzene, pyrimidine and thiophene as the C, N and S precursors.	—	ORR	> N-graphene & S-graphene	121
PN-graphene	Pyrolysis of graphene-dicyandiamide for N doping, and then pyrolysing it with phosphoric acid	—	ORR	> N-graphene	122

Therefore, the development of better synthetic strategies is still much needed. As can be seen from the catalytic efficiency shown in Table 1, all doped samples exhibit higher efficiency compared to un-doped graphene, demonstrating a great beneficial effect of doping on performance. Interestingly, all co-doped graphenes have shown better performance during the catalytic process than single element doped samples under the same conditions. This provides not only new insights on the underlying synergistic effect, but also a general strategy for the development of low cost and high performance metal-free doped graphene for catalysis.

Many characterization techniques including TEM, FTIR and XPS have been employed to study doped graphene. However, it is still difficult to obtain the precise image of the doped graphene. To the best of our knowledge, no work has been able to give the complete doped structures, and most of them only showed the concentration and bonding formats of these doped atoms. As we have discussed above, the doped structures are crucial for the catalytic properties. Therefore, more precise characterizations are required to completely understand the structure of doped graphene and its catalytic mechanism. For example, detailed surface characterizations with the help of

modern techniques such as scanning probing microscopy may help to display the detailed distribution of these doped atoms, even down to the single atom level.

Pristine graphene has a low chemical activity due to its uniform and symmetrical electronic structure. The doped elements can break the perfect π covalent bonds and induce local high electron/spin densities owing to the electronegativity differences, which contribute to its catalytic activity. In addition, the modifications at the edge of graphene sheets, such as the induced high strain of Se and O═S═O groups doped by S, can also facilitate the reactant's adsorption and enhance its chemical activity. Also, these doped groups may also be considered as active sites. For example, the oxygenated moieties on GO possess highly active chemical properties. Therefore, it is expected new metal-free catalysts could be prepared by doping with other elements. However, some problems remain to be resolved, and the catalytic investigations on these doped graphenes are still in the early stages and most of them are limited to ORR. For example, detailed comparisons among different doping elements should be performed, which will help to direct future studies. However, there is still little work involving side-by-side comparisons among doping of different elements in intrinsic graphene. Moreover, as different laboratories have reported different results, it is very difficult to draw any meaningful conclusions at the current stage. For example, N-graphene was found to show either higher[65] or lower[68] activity in ORR compared to commercial Pt catalyst. Also, the catalytic thermodynamics and kinetics are unclear and more detailed studies should be carried out. Single molecule technology may help to address this problem. Taking the N-doped graphene catalyzed reduction of Nip as an example, single layer graphene with high quality can be prepared by the CVD method and single foreign atom doping might be realized *via* STM or other technologies. One Nip molecule would be transferred to the doped site through precise manipulations. The processes of Nip adsorption, reduction of the nitro group and Amp desorption may be observed directly, demonstrating a precise catalytic process.

To fully resolve these problems, systematic theoretical simulations are also needed in addition to experiments, which may establish a clear relationship between doping and catalytic properties in the future. As for the co-doped models, much more research should be carried out to clearly understand the synergistic effects from the two doped elements.

Above all these, the practical applications of the doped graphene in more extreme conditions and under other influencing factors should be explored. For example, recovery is an inevitable issue for any catalyst. These doped graphenes can be prepared into 3D macroscopic structures by a gel method, which will make the recovery more convenient. However, this may affect their catalytic activities. As such, a more suitable and general recycling strategy is highly desired for practical catalytic applications. This field has enjoyed an explosive expansion in a rather short period of time. These new metal-free catalysts have already exhibited excellent properties in many catalytic reactions, and will certainly find more applications in other important and interesting catalytic reactions in the near future. Or even more creatively, these doped graphenes may enable new transformations that cannot be realized by metallic catalysts or cannot be realized at all before now. For example, some studies have demonstrated good CO_2 adsorption properties of N-doped graphene[123] and oxygen modified graphene.[124] We believe the metal-free catalytic transformations of CO_2 will be soon realized by doped graphene. In the meantime, mechanistic studies are crucial to help with the understanding of the current systems as well as the design of better catalysts. On September 19, 2012, the world's first graphene production line started construction in Ningbo City, Zhejiang Province in Southern China, with an anticipated annual production capacity of 300 tonnes. This project will be formally put into production in 2013 to produce high quality material, on a large scale, at low cost and in a reproducible manner, meaning the commercialization of graphene. This will ultimately open a way for graphene's exploitation in a wide spectrum of applications around the world.[125] With the improvement for large scale preparation and easy recovery, we expect that the doped graphene will be soon extended to industrial and commercial catalytic employment.

Acknowledgements

This work is supported by the National Natural Science Foundation of China (NSFC, 21071137, U1232211 and 21374108), Research Fund for the Doctoral Program of Higher Education of China (20133402120019) and the Recruitment Program of Global Experts.

Notes and references

1 B. F. Machado and P. Serp, *Catal. Sci. Technol.*, 2012, **2**, 54–75.
2 K. Gong, F. Du, Z. Xia, M. Durstock and L. Dai, *Science*, 2009, **323**, 760–764.
3 Y. Zheng, Y. Jiao, M. Jaroniec, Y. Jin and S. Z. Qiao, *Small*, 2012, **8**, 3550–3566.
4 S. Wang, E. Iyyamperumal, A. Roy, Y. Xue, D. Yu and L. Dai, *Angew. Chem., Int. Ed.*, 2011, **50**, 11756–11760.
5 L. Yang, S. Jiang, Y. Zhao, L. Zhu, S. Chen, X. Wang, Q. Wu, J. Ma, Y. Ma and Z. Hu, *Angew. Chem., Int. Ed.*, 2011, **50**, 7132–7135.
6 C. V. Rao and Y. Ishikawa, *J. Phys. Chem. C*, 2012, **116**, 4340–4346.
7 J. Zhang, X. Liu, R. Blume, A. Zhang, R. Schloegl and D. S. Su, *Science*, 2008, **322**, 73–77.
8 B. Frank, M. Morassutto, R. Schomaecker, R. Schloegl and D. S. Su, *ChemCatChem*, 2010, **2**, 644–648.
9 J. McGregor, Z. Huang, E. P. J. Parrott, J. A. Zeitler, K. L. Nguyen, J. M. Rawson, A. Carley, T. W. Hansen, J. P. Tessonnier, D. S. Su, D. Teschner, E. M. Vass, A. Knop-Gericke, R. Schloegl and L. F. Gladden, *J. Catal.*, 2010, **269**, 329–339.

10 A. Rinaldi, J. Zhang, B. Frank, D. S. Su, S. B. A. Hamid and R. Schloegl, *ChemSusChem*, 2010, **3**, 254–260.
11 J. Zhang, X. Wang, Q. Su, L. Zhi, A. Thomas, X. Feng, D. S. Su, R. Schloegl and K. Muellen, *J. Am. Chem. Soc.*, 2009, **131**, 11296–11297.
12 D. R. Dreyer, H. P. Jia and C. W. Bielawski, *Angew. Chem., Int. Ed.*, 2010, **49**, 6813–6816.
13 B. Li and Z. Xu, *J. Am. Chem. Soc.*, 2009, **131**, 16380–16382.
14 D. R. Dreyer, H. P. Jia, A. D. Todd, J. Geng and C. W. Bielawski, *Org. Biomol. Chem.*, 2011, **9**, 7292–7295.
15 H. Liu, Y. Liu and D. Zhu, *J. Mater. Chem.*, 2011, **21**, 3335–3345.
16 C. Berger, Z. Song, X. Li, X. Wu, N. Brown, C. Naud, D. Mayou, T. Li, J. Hass, A. N. Marchenkov, E. H. Conrad, P. N. First and W. A. de Heer, *Science*, 2006, **312**, 1191–1196.
17 C. Biswas and Y. H. Lee, *Adv. Funct. Mater.*, 2011, **21**, 3806–3826.
18 C. Huang, C. Li and G. Shi, *Energy Environ. Sci.*, 2012, **5**, 8848–8868.
19 M. Pumera and C. H. A. Wong, *Chem. Soc. Rev.*, 2013, **42**, 5987–5995.
20 C. Zhu and S. Dong, *Nanoscale*, 2013, **5**, 1753–1767.
21 E. Antolini, *Appl. Catal., B*, 2012, **123–124**, 52–68.
22 G. Liu, X. Li, J. W. Lee and B. N. Popov, *Catal. Sci. Technol.*, 2011, **1**, 207–217.
23 S. H. Hur and J. N. Park, *Asia-Pac. J. Chem. Eng.*, 2013, **8**, 218–233.
24 H. Wang, T. Maiyalagan and X. Wang, *ACS Catal.*, 2012, **2**, 781–794.
25 D. Chen, H. Feng and J. Li, *Chem. Rev.*, 2012, **112**, 6027–6053.
26 T. Szabo, O. Berkesi, P. Forgo, K. Josepovits, Y. Sanakis, D. Petridis and I. Dekany, *Chem. Mater.*, 2006, **18**, 2740–2749.
27 X. Kong and Q. Chen, *Acta Chim. Sin.*, 2013, **71**, 381–386.
28 A. Lerf, H. Y. He, M. Forster and J. Klinowski, *J. Phys. Chem. B*, 1998, **102**, 4477–4482.
29 C. Su, M. Acik, K. Takai, J. Lu, S.-J. Hao, Y. Zheng, P. Wu, Q. Bao, T. Enoki, Y. J. Chabal and K. P. Loh, *Nat. Commun.*, 2012, **3**, 1298–1306.
30 D. R. Dreyer and C. W. Bielawski, *Chem. Sci.*, 2011, **2**, 1233–1240.
31 H. P. Jia, D. R. Dreyer and C. W. Bielawski, *Tetrahedron*, 2011, **67**, 4431–4434.
32 H. P. Jia, D. R. Dreyer and C. W. Bielawski, *Adv. Synth. Catal.*, 2011, **353**, 528–532.
33 D. R. Dreyer and C. W. Bielawski, *Adv. Funct. Mater.*, 2012, **22**, 3247–3253.
34 D. R. Dreyer, K. A. Jarvis, P. J. Ferreira and C. W. Bielawski, *Polym. Chem.*, 2012, **3**, 757–766.
35 D. R. Dreyer, K. A. Jarvis, P. J. Ferreira and C. W. Bielawski, *Macromolecules*, 2011, **44**, 7659–7667.
36 Y. Song, K. Qu, C. Zhao, J. Ren and X. Qu, *Adv. Mater.*, 2010, **22**, 2206–2210.
37 X. Sun, Z. Liu, K. Welsher, J. T. Robinson, A. Goodwin, S. Zaric and H. Dai, *Nano Res.*, 2008, **1**, 203–212.
38 Y. Long, C. Zhang, X. Wang, J. Gao, W. Wang and Y. Liu, *J. Mater. Chem.*, 2011, **21**, 13934–13941.
39 Y. Pan, S. Wang, C. W. Kee, E. Dubuisson, Y. Yang, K. P. Loh and C. H. Tan, *Green Chem.*, 2011, **13**, 3341–3344.
40 H. Huang, J. Huang, Y. M. Liu, H. Y. He, Y. Cao and K. N. Fan, *Green Chem.*, 2012, **14**, 930–934.
41 D. W. Boukhvalov, D. R. Dreyer, C. W. Bielawski and Y. W. Son, *ChemCatChem*, 2012, **4**, 1844–1849.
42 F. Zeng, Z. Sun, X. Sang, D. Diamond, K. T. Lau, X. Liu and D. S. Su, *ChemSusChem*, 2011, **4**, 1587–1591.
43 L. Tang, Y. Wang, Y. Li, H. Feng, J. Lu and J. Li, *Adv. Funct. Mater.*, 2009, **19**, 2782–2789.
44 T. F. Yeh, J. M. Syu, C. Cheng, T. H. Chang and H. Teng, *Adv. Funct. Mater.*, 2010, **20**, 2255–2262.
45 H. C. Hsu, I. Shown, H. Y. Wei, Y. C. Chang, H. Y. Du, Y. G. Lin, C. A. Tseng, C. H. Wang, L. C. Chen, Y. C. Lin and K. H. Chen, *Nanoscale*, 2013, **5**, 262–268.
46 A. Dhakshinamoorthy, M. Alvaro, P. Concepcion, V. Fornes and H. Garcia, *Chem. Commun.*, 2012, **48**, 5443–5445.
47 A. Dhakshinamoorthy, M. Alvaro, M. Puche, V. Fornes and H. Garcia, *ChemCatChem*, 2012, **4**, 2026–2030.
48 S. Verma, H. P. Mungse, N. Kumar, S. Choudhary, S. L. Jain, B. Sain and O. P. Khatri, *Chem. Commun.*, 2011, **47**, 12673–12675.
49 A. V. Kumar and K. R. Rao, *Tetrahedron Lett.*, 2011, **52**, 5188–5191.
50 S. M. S. Chauhan and S. Mishra, *Molecules*, 2011, **16**, 7256–7266.
51 S. Tang and Z. Cao, *Phys. Chem. Chem. Phys.*, 2012, **14**, 16558–16565.
52 D. Wei, Y. Liu, Y. Wang, H. Zhang, L. Huang and G. Yu, *Nano Lett.*, 2009, **9**, 1752–1758.
53 D. Deng, X. Pan, L. Yu, Y. Cui, Y. Jiang, J. Qi, W. X. Li, Q. Fu, X. Ma, Q. Xue, G. Sun and X. Bao, *Chem. Mater.*, 2011, **23**, 1188–1193.
54 R. Wang, Y. Wang, C. Xu, J. Sun and L. Gao, *RSC Adv.*, 2013, **3**, 1194–1200.
55 X. Li, H. Wang, J. T. Robinson, H. Sanchez, G. Diankov and H. Dai, *J. Am. Chem. Soc.*, 2009, **131**, 15939–15944.
56 X. Wang, X. Li, L. Zhang, Y. Yoon, P. K. Weber, H. Wang, J. Guo and H. Dai, *Science*, 2009, **324**, 768–771.
57 N. Li, Z. Wang, K. Zhao, Z. Shi, Z. Gu and S. Xu, *Carbon*, 2010, **48**, 255–259.
58 D. Usachov, O. Vilkov, A. Grueneis, D. Haberer, A. Fedorov, V. K. Adamchuk, A. B. Preobrajenski, P. Dudin, A. Barinov, M. Oehzelt, C. Laubschat and D. V. Vyalikh, *Nano Lett.*, 2011, **11**, 5401–5407.
59 J. Bai, Q. Zhu, Z. Lv, H. Dong, J. Yu and L. Dong, *Int. J. Hydrogen Energy*, 2013, **38**, 1413–1418.
60 J. C. Carrero-Sanchez, A. L. Elias, R. Mancilla, G. Arrellin, H. Terrones, J. P. Laclette and M. Terrones, *Nano Lett.*, 2006, **6**, 1609–1616.
61 N. Q. Minh, *J. Am. Ceram. Soc.*, 1993, **76**, 563–588.

62 Y. Li, T. Li, M. Yao and S. Liu, *J. Mater. Chem.*, 2012, **22**, 10911–10917.
63 L. Qu, Y. Liu, J. B. Baek and L. Dai, *ACS Nano*, 2010, **4**, 1321–1326.
64 D. Geng, Y. Chen, Y. Chen, Y. Li, R. Li, X. Sun, S. Ye and S. Knights, *Energy Environ. Sci.*, 2011, **4**, 760–764.
65 L. Lai, J. R. Potts, D. Zhan, L. Wang, C. K. Poh, C. Tang, H. Gong, Z. Shen, J. Lin and R. S. Ruoff, *Energy Environ. Sci.*, 2012, **5**, 7936–7942.
66 Z.-H. Sheng, L. Shao, J.-J. Chen, W.-J. Bao, F.-B. Wang and X.-H. Xia, *ACS Nano*, 2011, **5**, 4350–4358.
67 K. R. Lee, K. U. Lee, J. W. Lee, B. T. Ahn and S. I. Woo, *Electrochem. Commun.*, 2010, **12**, 1052–1055.
68 Z. Luo, S. Lim, Z. Tian, J. Shang, L. Lai, B. MacDonald, C. Fu, Z. Shen, T. Yu and J. Lin, *J. Mater. Chem.*, 2011, **21**, 8038–8044.
69 Z. Lin, G. H. Waller, Y. Liu, M. Liu and C. P. Wong, *Nano Energy*, 2013, **2**, 241–248.
70 P. Wang, Z. Wang, L. Jia and Z. Xiao, *Phys. Chem. Chem. Phys.*, 2009, **11**, 2730–2740.
71 K. A. Kurak and A. B. Anderson, *J. Phys. Chem. C*, 2009, **113**, 6730–6734.
72 Y. Okamoto, *Appl. Surf. Sci.*, 2009, **256**, 335–341.
73 D. W. Boukhvalov and Y. W. Son, *Nanoscale*, 2012, **4**, 417–420.
74 L. Zhang and Z. Xia, *J. Phys. Chem. C*, 2011, **115**, 11170–11176.
75 L. Zhang, J. Niu, L. Dai and Z. Xia, *Langmuir*, 2012, **28**, 7542–7550.
76 H. Niwa, K. Horiba, Y. Harada, M. Oshima, T. Ikeda, K. Terakura, J. I. Ozaki and S. Miyata, *J. Power Sources*, 2009, **187**, 93–97.
77 T. Ikeda, M. Boero, S.-F. Huang, K. Terakura, M. Oshima and J. I. Ozaki, *J. Phys. Chem. C*, 2008, **112**, 14706–14709.
78 S. Yasuda, L. Yu, J. Kim and K. Murakoshi, *Chem. Commun.*, 2013, **49**, 9627–9629.
79 L. Yu, X. Pan, X. Cao, P. Hu and X. Bao, *J. Catal.*, 2011, **282**, 183–190.
80 J. A. Labinger and J. E. Bercaw, *Nature*, 2002, **417**, 507–514.
81 Y. Gao, G. Hu, J. Zhong, Z. Shi, Y. Zhu, D. S. Su, J. Wang, X. Bao and D. Ma, *Angew. Chem., Int. Ed.*, 2013, **52**, 2109–2113.
82 M. Nemanashi and R. Meijboom, *J. Colloid InterfaceSci.*, 2013, **389**, 260–267.
83 R. Fenger, E. Fertitta, H. Kirmse, A. F. Thunemann and K. Rademann, *Phys. Chem. Chem. Phys.*, 2012, **14**, 9343–9349.
84 N. Pradhan, A. Pal and T. Pal, *Colloids Surf., A*, 2002, **196**, 247–257.
85 P. Herves, M. Perez-Lorenzo, L. M. Liz-Marzan, J. Dzubiella, Y. Lu and M. Ballauff, *Chem. Soc. Rev.*, 2012, **41**, 5577–5587.
86 X. Kong, Z. Sun, M. Chen, C. Chen and Q. Chen, *Energy Environ. Sci.*, 2013, **6**, 3260–3266.
87 T. W. Chen, J. Y. Xu, Z. H. Sheng, K. Wang, F. B. Wang, T. M. Liang and X. H. Xia, *Electrochem. Commun.*, 2012, **16**, 30–33.
88 J. Long, X. Xie, J. Xu, Q. Gu, L. Chen and X. Wang, *ACS Catal.*, 2012, **2**, 622–631.
89 Y. Wang, Y. Shao, D. W. Matson, J. Li and Y. Lin, *ACS Nano*, 2010, **4**, 1790–1798.
90 Y. Shao, S. Zhang, M. H. Engelhard, G. Li, G. Shao, Y. Wang, J. Liu, I. A. Aksay and Y. Lin, *J. Mater. Chem.*, 2010, **20**, 7491–7496.
91 P. Wu, Y. Qian, P. Du, H. Zhang and C. Cai, *J. Mater. Chem.*, 2012, **22**, 6402–6412.
92 P. Wu, P. Du, H. Zhang and C. Cai, *Phys. Chem. Chem. Phys.*, 2013, **15**, 6920–6928.
93 Z. H. Sheng, X. Q. Zheng, J. Y. Xu, W. J. Bao, F. B. Wang and X. H. Xia, *Biosens. Bioelectron.*, 2012, **34**, 125–131.
94 Y. Xue, J. Liu, H. Chen, R. Wang, D. Li, J. Qu and L. Dai, *Angew. Chem., Int. Ed.*, 2012, **51**, 12124–12127.
95 A. Lherbier, X. Blase, Y. M. Niquet, F. Triozon and S. Roche, *Phys. Rev. Lett.*, 2008, **101**, 036808.
96 L. S. Panchokarla, K. S. Subrahmanyam, S. K. Saha, A. Govindaraj, H. R. Krishnamurthy, U. V. Waghmare and C. N. R. Rao, *Adv. Mater.*, 2009, **21**, 4726–4730.
97 Z. H. Sheng, H. L. Gao, W. J. Bao, F. B. Wang and X. H. Xia, *J. Mater. Chem.*, 2012, **22**, 390–395.
98 X. Kong, Q. Chen and Z. Sun, *ChemPhysChem*, 2013, **14**, 514–519.
99 P. A. Denis, R. Faccio and A. W. Mombru, *ChemPhysChem*, 2009, **10**, 715–722.
100 S. Yang, L. Zhi, K. Tang, X. Feng, J. Maier and K. Muellen, *Adv. Funct. Mater.*, 2012, **22**, 3634–3640.
101 Z. Yang, Z. Yao, G. Li, G. Fang, H. Nie, Z. Liu, X. Zhou, X. Chen and S. Huang, *ACS Nano*, 2012, **6**, 205–211.
102 I. Y. Jeon, S. Zhang, L. Zhang, H. J. Choi, J. M. Seo, Z. Xia, L. Dai and J. B. Baek, *Adv. Mater.*, 2013, **25**, 6138–6145.
103 J. Ji, G. Zhang, H. Chen, S. Wang, G. Zhang, F. Zhang and X. Fan, *Chem. Sci.*, 2011, **2**, 484–487.
104 E. Lam, J. H. Chong, E. Majid, Y. Liu, S. Hrapovic, A. C. W. Leung and J. H. T. Luong, *Carbon*, 2012, **50**, 1033–1043.
105 F. Liu, J. Sun, L. Zhu, X. Meng, C. Qi and F. S. Xiao, *J. Mater. Chem.*, 2012, **22**, 5495–5502.
106 C. Zhang, N. Mahmood, H. Yin, F. Liu and Y. Hou, *Adv. Mater.*, 2013, **25**, 4932–4937.
107 M. Latorre-Sánchez, A. Primo and H. García, *Angew. Chem., Int. Ed.*, 2013, **52**, 11813–11816.
108 P. A. Denis, *Chem. Phys. Lett.*, 2010, **492**, 251–257.
109 Z. W. Liu, F. Peng, H.-J. Wang, H. Yu, W. X. Zheng and J. Yang, *Angew. Chem., Int. Ed.*, 2011, **50**, 3257–3261.
110 Z. Jin, H. Nie, Z. Yang, J. Zhang, Z. Liu, X. Xu and S. Huang, *Nanoscale*, 2012, **4**, 6455–6460.
111 Z. Yao, H. Nie, Z. Yang, X. Zhou, Z. Liu and S. Huang, *Chem. Commun.*, 2012, **48**, 1027–1029.
112 Y. Chen, B. Gao, J.-X. Zhao, Q.-H. Cai and H.-G. Fu, *J. Mol. Model.*, 2012, **18**, 2043–2054.

113 Y. Zhao, W. F. Chen, C. F. Yuan, Z. Y. Zhu and L. F. Yan, *Chin. J. Chem. Phys.*, 2012, **25**, 335–338.
114 Z. S. Wu, A. Winter, L. Chen, Y. Sun, A. Turchanin, X. Feng and K. Muellen, *Adv. Mater.*, 2012, **24**, 5130–5135.
115 Y. Feng, F. Li, Z. Hu, X. Luo, L. Zhang, X. F. Zhou, H. T. Wang, J. J. Xu and E. G. Wang, *Phys. Rev. B: Condens. Matter Mater. Phys.*, 2012, **85**, 155454.
116 S. F. Huang, K. Terakura, T. Ozaki, T. Ikeda, M. Boero, M. Oshima, J. I. Ozaki and S. Miyata, *Phys. Rev. B: Condens. Matter Mater. Phys.*, 2009, **80**, 235410.
117 S. Wang, L. Zhang, Z. Xia, A. Roy, D. W. Chang, J. B. Baek and L. Dai, *Angew. Chem., Int. Ed.*, 2012, **51**, 4209–4212.
118 Y. Zheng, Y. Jiao, L. Ge, M. Jaroniec and S. Z. Qiao, *Angew. Chem., Int. Ed.*, 2013, **52**, 3110–3116.
119 X. Fan, W. T. Zheng and J. L. Kuo, *RSC Adv.*, 2013, **3**, 5498–5505.
120 J. Liang, Y. Jiao, M. Jaroniec and S. Z. Qiao, *Angew. Chem., Int. Ed.*, 2012, **51**, 11496–11500.
121 J. Xu, G. Dong, C. Jin, M. Huang and L. Guan, *ChemSusChem*, 2013, **6**, 493–499.
122 C. H. Choi, M. W. Chung, H. C. Kwon, S. H. Park and S. I. Woo, *J. Mater. Chem. A*, 2013, **1**, 3694–3699.
123 V. Chandra, S. U. Yu, S. H. Kim, Y. S. Yoon, D. Y. Kim, A. H. Kwon, M. Meyyappan and K. S. Kim, *Chem. Commun.*, 2012, **48**, 735–737.
124 Y. Liu and J. Wilcox, *Environ. Sci. Technol.*, 2012, **46**, 1940–1947.
125 http://investorintel.com/graphite-graphene-intel/the-revolutionary-era-of-industrial-scale-graphene-is-coming/.

